Journal of Institute of Science and Technology, 27(1), 149-158 (2022)
ISSN: 2467-9062 (print), e-ISSN: 2467-9240
https://doi.org/10.3126/jist.v27i1.46717

Research Article

FIRST-PRINCIPLES STUDY OF ELECTRONIC AND MAGNETIC PROPERTIES OF TWO-DIMENSIONAL HEXAGONAL BORON NITRIDE DOPED WITH GERMANIUM AND TIN ATOMS

Dipak Adhikari[1,2], Jeewan Panthee[1], Saurabh Lamsal[1] , Kapil Adhikari[2.3], Narayan Prasad Adhikari[1], Nurapathi Pantha[1]
[1]Central Department of Physics, Tribhuvan University, Kirtipur, Kathmandu, Nepal
[2]Department of Physics, Prithvi Narayan Campus, Tribhuvan University, Pokhara, Nepal
[3]Gandaki University, Pokhara, Nepal
**Corresponding author: mrnurapati@gmail.com*
(Received:** December 09, 2021; **Revised:** May 31, 2022; **Accepted:** June 30, 2022**)

ABSTRACT
For the study of geometrical structure, stability, and electronic and magnetic properties of Germanium and tin-doped two-dimensional hexagonal boron nitride (h-BN), First-principles calculations have been carried out. Plane-wave pseudo-potential method in association with the density functional theory (DFT) framework used in Quantum ESPRESSO codes has been implemented to perform the calculations. A 3×3 supercell size substitutional doping of a single Boron or Nitrogen atom was carried out for the study. Pristine h-BN showed non-magnetic behavior with comprehensive gap material having an indirect band gap of 4.64eV. The doping effect of Ge and Sn atoms at the B-site was energetically more favorable than N-site. The defected h-BN sheet was found to be severely distorted with remarkable alteration in bond length and angles around the defected sites. Ge doped h-BN showed semiconducting properties with a reduced band gap in comparison to the insulating nature of pristine h-BN, whereas half metallicity was noticed in Sn doped h-BN system. Both the systems showed a magnetic moment of 1.0 μB.

Keywords: Band gap, density functional theory, formation energy, half metallicity

INTRODUCTION
Boron Nitride is an III-V compound that has been studied in detail for its wide range of interesting features like insulating, semiconducting, half metallicity, etc. after doping. Both theoretical and experimental studies have been done on different crystalline forms of BN (Xu & Ching, 1993; MacNaughton *et al*., 2005; Lin & Connell, 2012; Cassabois *et al*., 2016). There are four polymorphic modifications of BN, namely cubic (c-BN), hexagonal (h-BN), wurzite (w-BN), and rhombohedral (r-BN). Two of them, named c-BN and w-BN, have a sp^3 hybrid bond between B and N, a tetrahedral structure with diamond-like hard phases whereas h-BN and r-BN have an sp^2 hybridized bond (Azevedo *et al*., 2009; Lin & Connell, 2012; Xu *et al*., 2013). Bulk h-BN is the stable polymorph at room temperature and ambient pressure, which is structurally analogous and isoelectronic to graphite. After the isolation of graphene in 2004 and the revelation of its extraordinary properties (Novoselov *et al*., 2004), other 2D systems have gained significant scientific attention (Xu *et al*., 2013; Berseneva *et al*., 2013). Among them, a two-dimensional sheet of h-BN, consisting of alternating boron and nitrogen atoms in a honeycomb arrangement of a basal plane can be extracted because of weak van der Waals interaction. The lattice parameters for h-BN are in the order of a = b = 2.50 A° and c = 6.66 A° (Ooi *et al*., 2005). Two-dimensional h-BN has been produced by techniques like micromechanical cleavage, high-energy electron beam irradiation of BN particles, chemical decomposition, and catalytic chemical vapor deposition (CVD) (Azevedo *et al*., 2009; Lin & Connell, 2012; Berseneva *et al*., 2013). Although not as intriguing electronically as graphene, h-BN has other superior properties like hardness, high melting point, low dielectric constant, and large band gap (Lin & Connell, 2012). So monolayer h-BN is a material with potential applications in ultraviolet photonics (Cassabois *et al*., 2016), as insulating substrates in heterostructures (Geim & Grigorieva, 2013) as wide band semiconductors (Liu *et al*., 2014) for catalytic actions (Lin *et al*., 2013; Sinthika *et al*., 2014), and in hybrid BNC structures (Berseneva *et al*., 2013) working in extreme conditions. Graphene burns at around 800K whereas h-BN withstands a temperature of 1000K (Lin *et al*., 2013).

There have been many theoretical and experimental studies on the electronic properties of bulk h-BN (Xu & Ching, 1993; Liu *et al*., 2003; MacNaughton *et al*., 2005). But very few agree on the band gap and its nature. Experimentally, h-BN crystals are found to have different band gaps ranging between 3.6 - 7.1eV (Liu *et al*., 2003). DFT calculations in the generalized gradient approximation (GGA) employing Perdew-Burke-Ernzerhof (PBE) functional for electron exchange-correlation potential conducted in 2012 found that monolayer h-BN has an indirect band gap of 4.56eV (PBE functional underestimates the band gap) (Azevedo *et al*., 2009). Further, bulk h-BN and 2D h-BN can have a difference in their band gap. Using hybrid functionals and the Green's

function quasiparticle (GW) methods it has been observed that band gaps for bulk and monolayer h-BN differ by more than 0.5eV (Berseneva *et al.*, 2013). The available literature suggests to us that the band gap of h-BN is not yet established accurately. Monolayer h-BN has the same number of electrons (Liu *et al.*, 2003) in a primitive cell as in graphene but unlike graphene, it is chemically and electronically inert. Recent studies have focused on substitutional and interstitial doping of h-BN with group IV elements and metals in search of the potential use of such an impure system in gaseous adsorption, catalytic actions, and semiconducting applications (Lin *et al.*, 2013; Sinthika *et al.*, 2014; Cassabois *et al.*, 2016). First-principles study of 32 atom h-BN sheet with different numbers of Carbon impurities showed that new states due to defects exist in the region of pristine h-BN band gap (Berseneva *et al.*, 2013). Defect configurations and local bond lengths around defects are sensitive to their charge states due to which the defect formation energies for substitutional doping of B or N can be vastly different (Azevedo *et al.*, 2009). As per the study conducted on Si-doped h-BN sheet, it is understood that formation energy (E_F) for Si_B defect (One B atom replaced by one Si atom) is 4.80eV and that for Si_N defect (One N atom replaced by one Si atom) is 10.22eV. Doping can also introduce some magnetic moment to pristine h-BN sheets (Liu *et al.*, 2014).

The theoretical investigations of C and Si-doped h-BN monolayer find remarkable changes in the electronic, magnetic, and transport properties of the pristine monolayer of h-BN (Azevedo *et al.*, 2009; Liu *et al.*, 2014). First-principles study of the h-BN sheet by doping with C and Si has focused on stability, geometry, and electronic/magnetic properties of such impure h-BN in comparison to pure h-BN (Berseneva *et al.*, 2013; Liu *et al.*, 2014). The prospect of doping h-BN with a group IV element is appealing for computational research. In this work, pristine two-dimensional h-BN (18 atom sheet) and the doped h-BN sheet with Ge and Sn atoms have been studied for structural changes, stability, and electronic/magnetic properties.

COMPUTATIONAL METHOD

First-principles calculations to study geometrical structure, stability, and electronic and magnetic properties of germanium and tin-doped h-BN and pristine h-BN have been performed in the framework of density functional theory. The crystal structure was visualized by using software XCrySDen (Kokalj, 1999) and PWscf (Plane-Wave self-consistent field) calculations were conducted in the Quantum ESPRESSO package (Giannozzi *et al.*, 2009; Giannozzi *et al.*, 2017). The ultra-soft pseudopotential was used for core and valence electron interaction, with Generalized Gradient Approximation for exchange-correlation energy. An iterative approach was used in the PWscf package. A 'Plain' mixing mode was used for mixing of charge in a subsequent iteration. Further, the 'David' approach of diagonalization was used to diagonalize the Kohn-Sham states as required in total energy calculation. A mixing factor of 0.7 was used. The total energy convergence threshold was set to 10^{-4}Ry(1 Rydbergs = 13.6 eV) and the force convergence threshold was set to 10^{-3}Ry/Bohrs (1 Bohr=0.53$A°$). For self-consistent total energy calculations, the Brillouin zone was sampled in k-space using the Monkhorst-Pack scheme with an appropriate number of k-points determined from the convergence tests. For geometrically optimized structure, 'relax' calculation was conducted under Broyden-Fletcher-Goldfarb-Shanno (BFGS) scheme until the energy difference between two consecutive 'scf' calculations was less than 10^{-4}Ry.

With a total energy convergence threshold of 10^{-4}Ry, the optimized cutoff kinetic energy value for scf calculations was chosen to be 40 Ry (1Ry=13.6eV). Taking a primitive cell, the optimal size of k-point mesh was chosen to be $12 \times 12 \times 1$ and the optimized primitive cell parameter was taken to be a=b=4.74 Bohrs. A hexagonal lattice with c=20$A°$ (nearly three times larger than that of bulk h-BN, 6.66 $A°$ (Xu & Ching, 1993)) was taken along the z-direction to avoid interlayer interaction. Our study was conducted on a 3×3 supercell of pristine 2D hexagonal h-BN obtained from optimized primitive cell dimensions. The impurity atoms Ge/Sn were doped on the same sized (3×3) h-BN sheet. The doped systems were allowed to relax with a force convergence threshold $= 10^{-3}$ Ry/Bohrs. For the supercell size calculations, a $4 \times 4 \times 1$ k-points grid was used except for nscf calculations (an $8 \times 8 \times 1$ k-points grid was used for nscf calculations).

RESULTS AND DISCUSSION

Geometry and formation energy of doped systems

The 3×3 supercell of pure h-BN monolayer contains nine boron and nine nitrogen atoms forming a hexagonal honeycomb lattice as in figure 1. The optimized lattice parameters for this supercell are found to be a = b = 14.19 Bohrs (7.52 $A°$).

Substitutional doping of monolayer h-BN was conducted by replacing a B (or N) atom with a Ge/Sn atom in an optimized 3×3 supercell of the pure h-BN sheet. Because of the very large size compared to B or N atoms, Ge and Sn atoms were expected to form a stable configuration outside of the h-BN plane. The relaxed structures of the doped system were found to possess a peculiar convex geometry around Ge/Sn atom and the in-plane symmetry of the monolayer is broken as shown in figure 2.

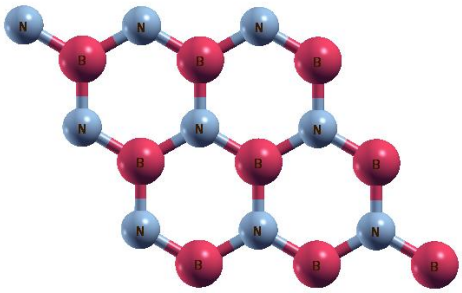

Figure 1: Supercell of 3×3 h-BN sheet with B and N atoms in a hexagonal lattice

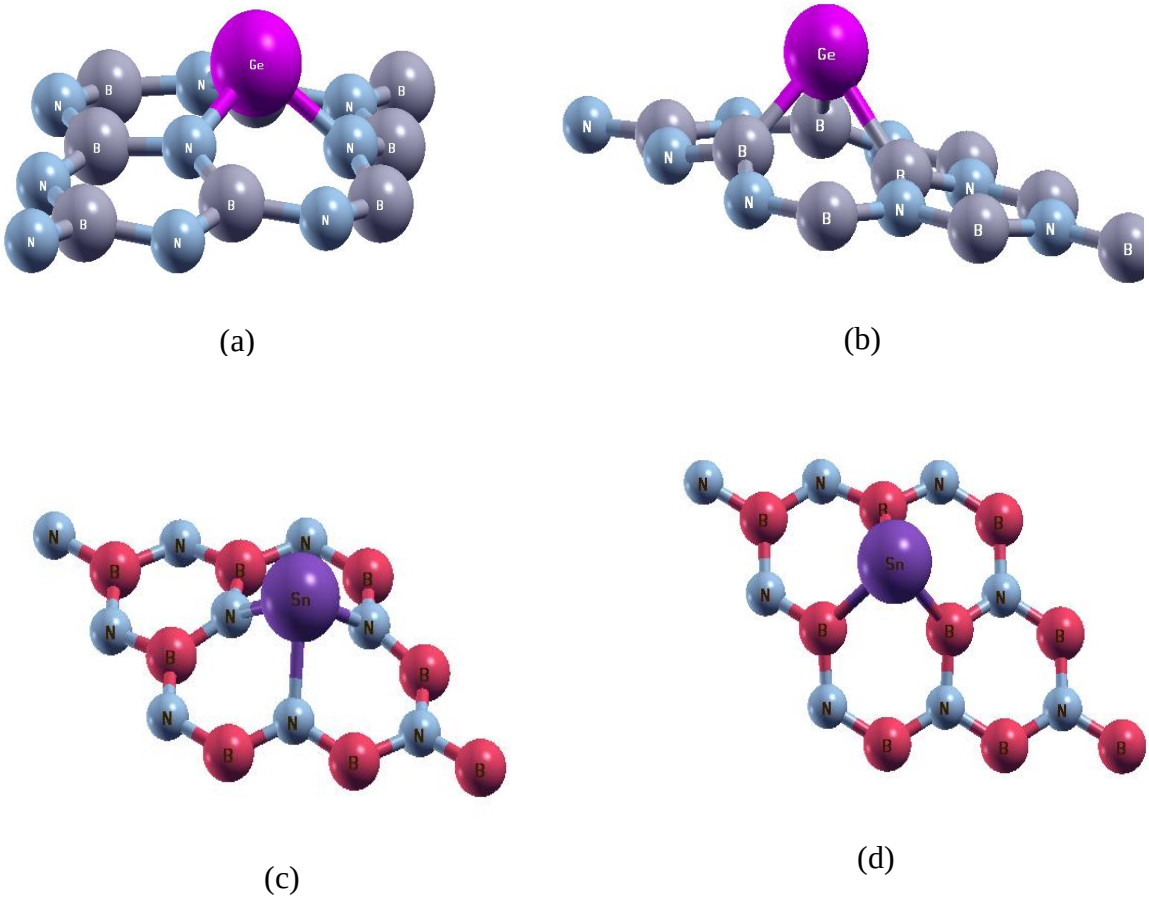

Figure 2: Relaxed structures of Ge and Sn doped h-BN sheet (a) Ge doped at B site (Ge_B) (b) Ge doped at N site (Ge_N) (c) Sn doped at B site (Sn_B) (d) Sn doped at N site (Sn_N)

For the Ge_B defect (Fig. 2a) the dopant Ge is bonded to three nearest N-atoms with equivalent three Ge-N bond lengths 1.82 A° in the h-BN sheet. The value is much larger than the usual B-N sp^2 bonds (1.45 A°) of a pure h-BN sheet. The average N-Ge-N bond angles are 98.60°. The deformation in structure causes the Ge atom to be protruded outwardly by 1.08 A° from the h-BN layer. The structural change when doping of Ge is done at the N site (Ge_B defect) is similar. Here Ge atom forms bonds to three nearest B atoms with bond lengths of about 2.10 A° and B-Ge-B bond angles differing from each other with values

of about $76°, 77°,$ and $83°$ respectively as shown in figure 2b. The Ge atom is 1.63 $A°$ above the h-BN plane. Two doped systems (by Ge atom at B and N sites) have different degrees of distortion due to differences in the chemical properties of the replaced atoms. The bond lengths pertaining to Ge substitution at the B site are shorter than Ge at the N site due to the higher electronegativity of N.

Similarly for Sn doping, the impurity atom is farther from the plane in Sn_N than in Sn_B. In Sn_B (Fig.2c), Sn lies 1.97 $A°$ above the plane whereas, in Sn_N (Fig.2d), it lies 2.18 $A°$ above the plane. These values are significant and comparable to the size of lattice parameter (a) of the primitive cell. Accordingly, the average bond angles N-Sn-N ($78.6°$) and B-Sn-B ($70°$) are significantly different. Compared to Ge doping, the geometry is furthermore distorted in Sn doping. The nearest-atoms bond lengths Sn-N (for Sn_B) and Sn-B (Sn_N) were observed to be respectively 2.16 $A°$ and 2.35 $A°$. From these observations, we understand that Ge or Sn have slightly more affinity to the vacancy at the B site and doping is more viable than that at the Nitrogen site. We can reaffirm this conclusion with the help of formation energy (E_{df}) calculations. The defect formation energy for Ge/Sn doping into the h-BN sheet can be calculated with equation (1) (Liu *et al.*, 2014),

$$E_{df} = (E_i - E_p) - (E_1 - E_2) \quad \ldots\ldots\ldots\ldots (1)$$

where E_i is the total energy of an impure(doped) h-BN sheet, E_p is the total energy of a pristine h-BN sheet, E_1 is the energy of a single dopant atom and E_2 is the energy of a single B or N atom. The energy of isolated Sn, B, and N atoms were calculated using an isolated system of single atoms kept in a large cubical box of dimension $8.87A°$. The formation energy (E_{df}) in Ge_N defect is approximately equal to 12.28 eV. The value is much larger than that of the Ge_B defect 7.75 eV. This suggests that the Ge substitution at the N site in the monolayer of h-BN will be an energetically more demanding process. In a similar way, E_{df} for Sn_B is 9.34eV which is considerably less than 12.97eV, the formation energy of Sn_N. Thus, the doping of Ge or Sn at the B site is more energetically favorable than at the N site. A previous study found a similar pattern of defect formation energy for Si (4.80eV for Si_B and 10.22eV for Si_N) in monolayer h-BN (Liu *et al.*, 2014). The larger values of formation energies might be due to the bigger atomic size of Ge or Sn atom than Si. For both Ge and Sn doping, replacing a Boron atom is more favorable than that of a Nitrogen atom from the h-BN sheet.

Electronic properties

In this section electronic structure of pristine h-BN, Ge doped h-BN, and Sn doped h-BN on the basis of spin-polarized band structure and the density of states calculations, have been discussed. The band structure of pristine h-BN was calculated after specifying the 100 k-points along a closed path through highly symmetric points (K-Γ-M-K) in the irreducible Brillouin zone. Computation of density of states (DOS) was carried out using an $8 \times 8 \times 1$ Γ centered Brillouin zone sampling. Both the band structure and density of states calculations show that pure h-BN is comprehensive gap material (Fig. 3a). It was observed that a direct band gap of magnitude 4.64eV at Γ point. The value of the band gap agrees well with the values in published literature (Barcza et al., 2021) while the nature of the band gap is in disagreement with the indirect nature asserted in the study using the PBE functional which may be due to our differences in computational method and model applied. The band structure is symmetric with respect to the spin states of electrons.

Ge doped h-BN sheet (Ge_B and Ge_N)

To gain deeper insights into the electronic properties of the Ge-doped h-BN sheets, the band structure of Ge_B and Ge_N systems are plotted by defining the high symmetry points (K, Γ, M, K) on the edge of the irreducible Brillouin zone. The band structure of Ge doped at B-site of 3×3 supercell of the h-BN sheet for up and down spin states is shown in figure 4a.

If the band structure around the Fermi level is compared with that of pure h-BN, it is found that there is a significant reduction in the band gap of the h-BN sheet after doping with germanium at the boron site of the h-BN monolayer. The combined band structure for up and down spin states of Ge-doped at the B-site of the h-BN sheet is shown in figure 4b.

The band gap of Ge-doped h-BN is found to be 2.88 eV which is less than that of pure h-BN (4.64 eV). Since maxima of the valence band and minima of the conduction band are both located at the M-point point of BZ, the band gap is direct at M-point. The reduction of the band gap is due to additional Ge atoms. Comparing the number of valance electrons of boron (3-valance electrons) and germanium (4-valance electrons), it is possible to infer that the germanium atom behaves like a donor impurity and causes the redistribution of electron density. It increases the energy of such electron to a state inside the energy gap, around the Fermi level.

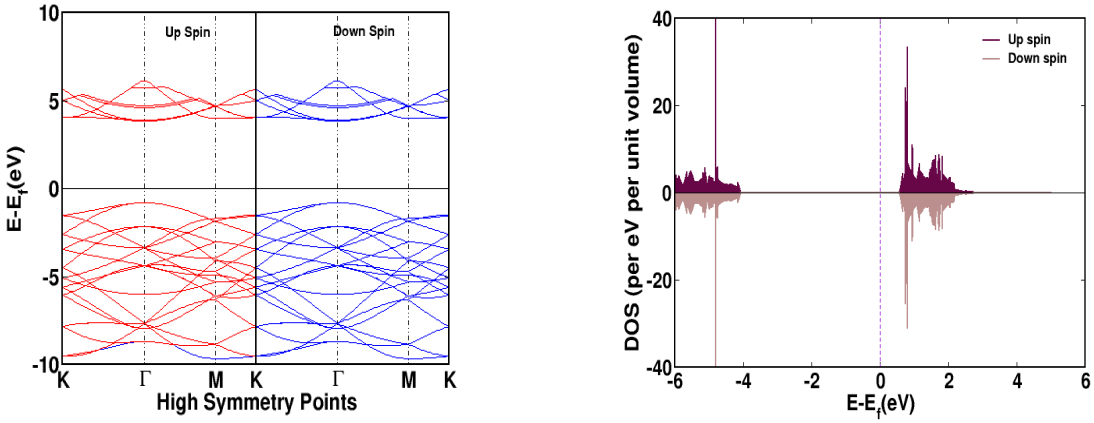

(a) (b)

Figure 3: (a) Band structure of pristine h-BN, $E_F = -3.28eV$ (b) Spin polarised density of states of pristine h-BN

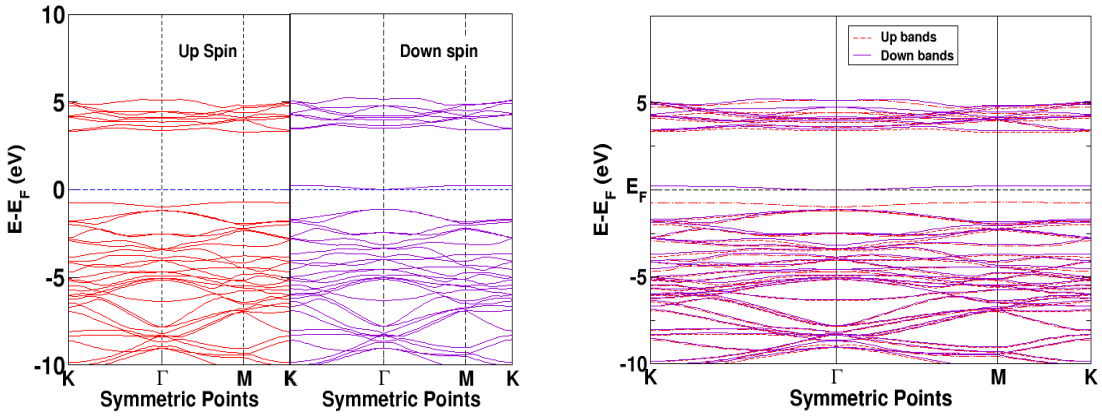

(a) (b)

Figure 4: (a) Band structure of h-BN with Ge atom at B site(Ge_B) (b) Combined band structure

With the description above, it can be inferred that the increasing concentration of Ge_B defects cause the occurrence of an insulator-metal transition. On the other hand, when a nitrogen atom is substituted by a germanium atom (creating Ge_N defect), the calculated energy gap is found to be 1.65 eV (indirect at Γ-M point, figure 5). There is a significant reduction of the gap by 2.91 eV from the pure band gap. Here the band gap represents the regime of the semiconductor and infers that substitutional doping of the germanium atom changes an insulator (h-BN) to a semiconductor. The substitution of N by Ge behaves as if the impurity atom is the acceptor one and the Fermi level shifts downwards. To identify the contribution of orbitals in the electronic states of the doped system, we analyzed the DOS and Partial DOS as shown in figures 6 and 7.

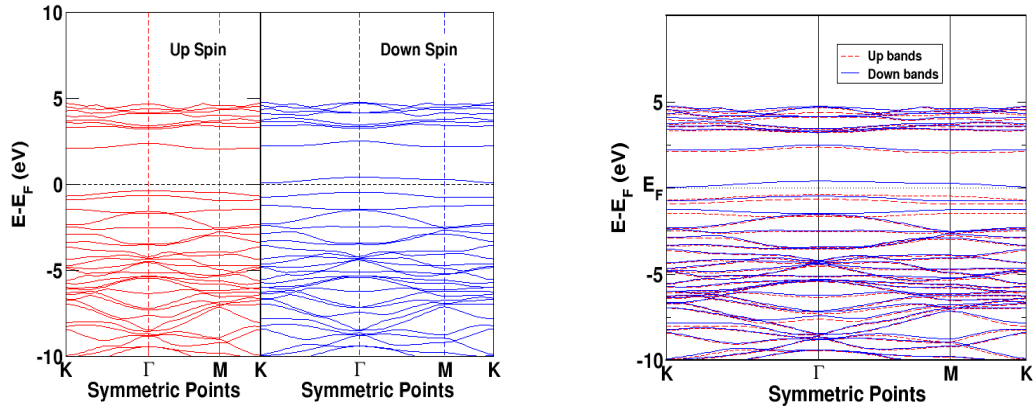

Figure 5: (a) Band structure of h-BN with Ge atom at N site (Ge_N) (b) Combined band structure.

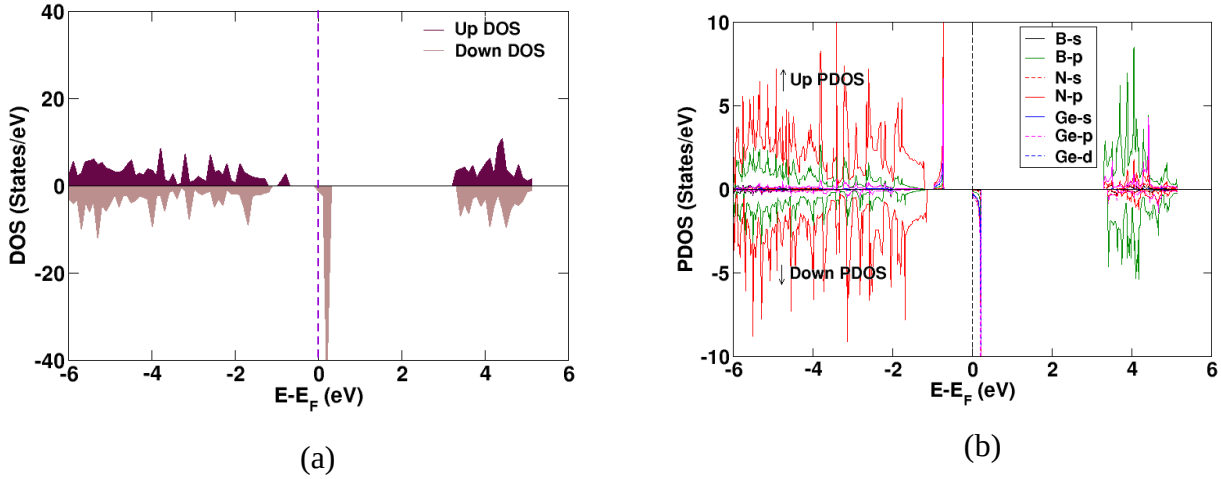

Figure 6: (a) Spin-polarized density of states of Ge_B (b) Projected DOS for Ge_B

For Ge_B it is observed that the DOS of both up spin and down spin states shows a certain band gap. The overlapping of down spin states with the Fermi level is within the error bar. Therefore, the material behaves as a semiconductor with a band gap of 2.88 eV. The partial density of states, i.e., contribution of different atoms, and their orbitals, are presented in figure 6b. This shows majority contribution in DOS is due to 2p orbitals of B and N and 4p orbital of Ge. Near Fermi level up and down spin DOSs for Ge_B system is dominated by 4p orbital of Ge and 2p orbitals of N respectively. For Ge_N, the picture is similar. Both up and down spin DOS shows reduced band gap values, and the material behaves as a semiconductor.

Sn doped h-BN sheet (Sn_B and Sn_N)

Due to the presence of substitutional impurity like Sn in h-BN, the structure is severely distorted (Figs. 2c and 2d) and thus affects the ionic potential around defected sites. This changes spin-polarized scf, DOS, and Projected DOS (for the contribution of single atom orbitals) structures in doped systems (Sn_B and Sn_N) with reference to the pristine one. The results are consistent with the previous study of Si-doped h-BN sheets (Liu et al., 2014).

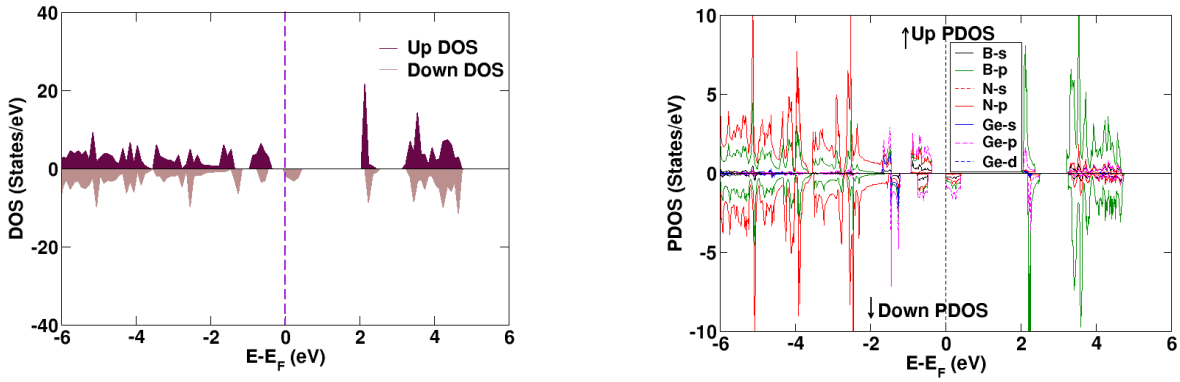

(a) (b)

Figure 7: (a) Spin-polarized density of states of Ge_N (b) Projected DOS for Ge_N

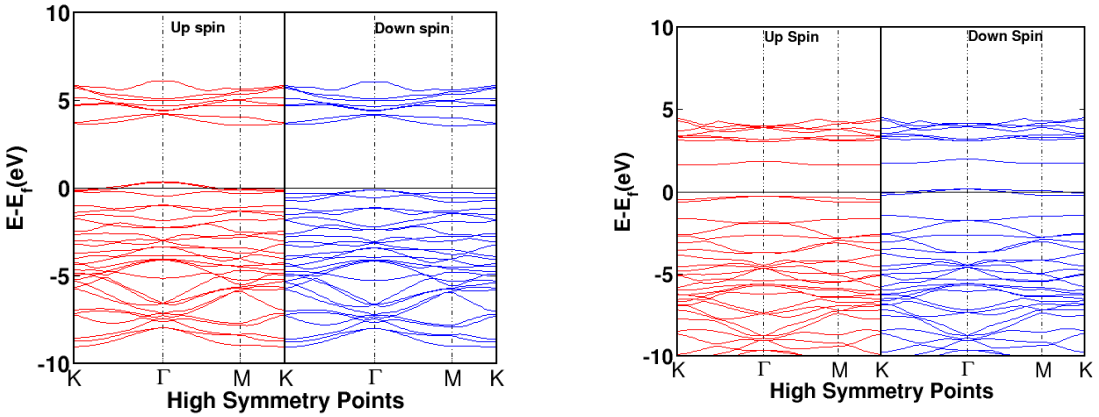

(a) (b)

Figure 8: (a) Band structure of h-BN with Sn atom at B site(Sn_B) (b) Band structure of h-BN with Sn atom at N site(Sn_N)

From Fig. 8(a), it is observed that for up spin electrons in Sn_B the Fermi level lies just within the valence band with the highest unoccupied states lying 0.29eV above the Fermi level. But for down spin electrons the Fermi level nearly touches the valance band. These new states are present due to the effect of doping. Since bands around the Fermi level are significantly different from those in pristine 3×3 h-BN (Fig. 3) we can say that energy levels of valance orbitals (s and p) of B and N are also changed around the Fermi level. From Fig. 8(a), we see that when Sn is doped in an h-BN sheet, the system gains half-metallic character (metallic up spin and semiconducting down spin). The Fermi level of the doped system is found to be slightly decreased (-3.40 eV) compared to that of the pristine 3×3 h-BN sheet (-3.28eV). This slight decrease in Fermi energy level might be due to the acceptor-like character brought by the presence the of Sn atom. Compared with the band structure of pristine h-BN (Fig. 3) we can understand the new states around the Fermi level due to the Sn atom. The total DOS and Projected DOS plots are shown in Fig. 9

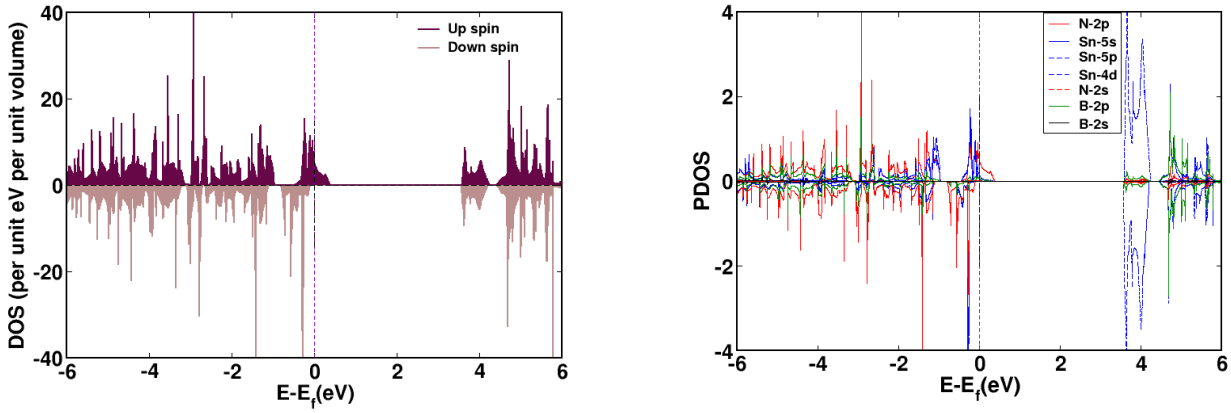

(a) (b)

Figure 9: (a) Spin polarized density of states of Sn_B, (b) Projected DOS for Sn_B

The DOS for low energy states is almost symmetrical. Difference in DOS gradually increases and becomes significant around the Fermi level. It can be seen that for up spin there are many vacant states above Fermi energy which gives half metallicity to our system. From the Projected DOS calculations, it can be seen that h-BN sheet doped with Sn atom at B site, the available states around Fermi level are largely due to N and Sn atom. The s and p orbitals of the Sn atom are sp^2 hybridized and thus forming three covalent bonds with p-orbitals of the N atom around the defected site. The d-orbital of the Sn atom is empty, and the s-orbital of the N atom remains intact as seen from the non-existent DOS for d-orbital (Sn atom) and s-orbital (N atom). So, it is concluded that the Sn atom forms a stable system with the interaction between p-orbitals of the N atom and sp^2 hybrid orbitals of the Sn atom. This is understandable since we have replaced a Boron atom with a Sn atom and the Sn atom interacts with the nearest available N atoms.

The band structure of Sn_N system (Fig. 8(b))shows that the states around 2eV below the Fermi level are not significantly altered in comparison to the band structures of pristine h-BN (Fig. 3) and band structure of Sn doped h-BN at B site (Fig.8 (a)). However, an interesting phenomenon is observed that Sn_N is semiconducting in nature for up spin electrons and metallic in nature for down spin electrons. The levels around the Fermi level are due to the Sn atom. The Fermi level of the doped system Sn_N is shifted upwards. So, we can say from our calculations that doping h-BN with Sn at the N site possibly brings n-type conductivity in up spin electrons. The aforementioned results are further evident from the DOS and Projected DOS calculations (Fig. 10). There is significant density above the Fermi level for down spin whereas for up spin the vacant states density is very less and far from the Fermi level. The Fermi energy for this system is -2.27eV, which is nearly 1eV more than that for pristine h-BN. From this observation we can conclude that doping of Sn at N-site acts as donor. Comparison with total DOS of pristine h-BN (Fig. 3b) it can be observed that the lower states are symmetrical in terms of density whereas states around the Fermi energy are massively affected. This indicates possible magnetisation in our doped system Sn_N.

Magnetic properties

The magnetic moment of a system is related to symmetry of up spin and down spin DOS of the system. The total magnetic moment is given by $\mu = m\,\mu_B$, where m is the number of unpaired electrons and μ_B is the magnetic moment of single electron. It is called Bohr magneton. 'm' can be obtained by counting the electrons in the spin 'up' and spin 'down' sub bands.

$$m = \int_{-\infty}^{+\infty}\left(D_{\uparrow}(\epsilon) - D_{\downarrow}(\epsilon)\right)d\epsilon \quad \ldots\ldots\ldots (2)$$

This equation shows if DOS for spin-up electrons and spin-down electrons are exactly same, i.e., symmetrical, system will be non-magnetic.

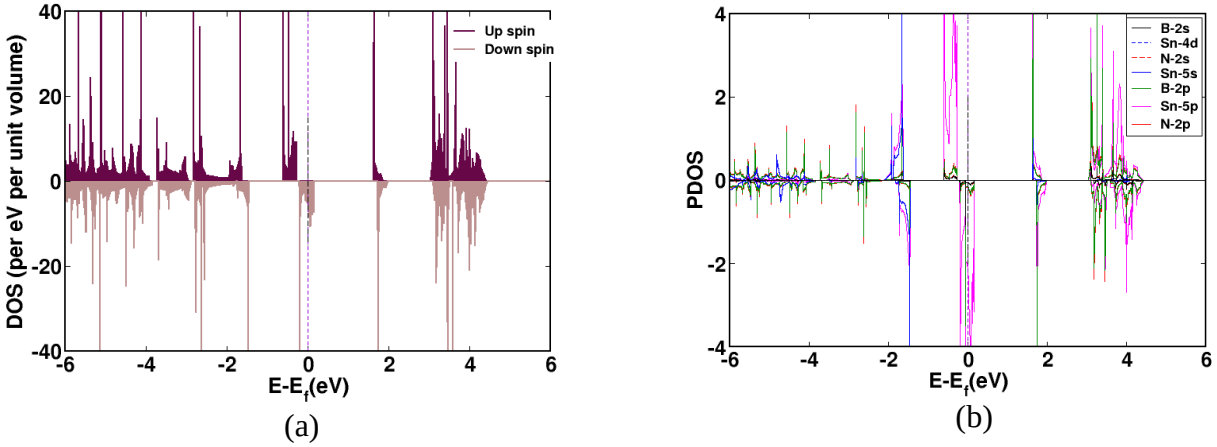

Figure 10: (a) Spin polarized density of states of Sn_N (b). Projected DOS for Sn_N

Under relaxation based on DFT using QE code, we find Ge doped at B side of h-BN spin polarized with a magnetic moment of about 1.00 μ_B, which can be confirmed by the DOS plot (Fig. 6a). Similar to the case for Ge_B defect, upon doping of Ge atom, the DOS of h-BN monolayer sheet at N-site also changes to non-symmetrical (Fig. 7a). This type of asymmetric nature of DOS indicates the magnetic nature of Ge doped h-BN system and is quantified as $1.00\ \mu_B$. This value of magnetic moment was seen to be similar to that for silicon doped h-BN system calculated by Liu *et al.* (Liu *et al.*, 2014). The magnetic moment mainly originates from the contribution of Ge impurity.

Similarly in case of Sn doped at B-site of 3×3 h-BN sheet (Sn_B),the asymmetric density of states implies certain magnetic moment is associated with the system. Results obtained from spin polarised scf calculations show that the doping of Sn atom at Boron site induces total magnetization of $-1\mu_B$ per unit cell . The magnetization is observed due to redistribution of electronic states in the doped system which brings difference in density of states for two different spin states. Likewise in case of Sn doped at N-site of h-BN sheet (Sn_N), the asymmetric density of states implies certain magnetic moment associated with the system. Results obtained from spin polarized scf calculations show that the doping of Sn atom at Nitrogen site induces total magnetization of $+1\mu_B$ per unit cell.

CONCLUSIONS

Two atoms (Sn and Ge) were separately doped at B and N sites of h-BN to study their various properties by using the first-principles method of calculations. The doped/ defected systems show that the Sn and Ge atoms at both the sites lead to a large distortion in the sheet. The distortion in geometry includes changes in angles and bond lengths of impurity atoms with nearest B (or N) atoms. The formation energy for Ge_N , Ge_B, Sn_N and Sn_B were found to be 12.28 eV, 7.75 eV, 12.97 eV and 9.34 eV respectively. The larger formation energy implies the lesser stability of the system, and hence doping at B site is more preferable than at N sites. The band structure of doped systems was also changed with respect to pristine h-BN monolayer (4.56 eV). Upon the doping of Ge, the system gains semiconducting character whereas doping of Sn makes h-BN half metallic. Further the impurity atoms induce magnetism of magnetic moment $1\mu_B$ in both the cases (for Ge and Sn atoms).

The work can be extended with varying concentration of impurity atom/s. Further, there are promising signs of half-metallicity and n-type material on doping of group IV atoms. Sensing and storage of gaseous molecules in doped h-BN is another possible field to explore.

ACKNOWLEDGEMENTS

The authors acknowledge TWAS (The World Academy of Sciences) research grants RG 20-316 for computational facility.

AUTHOR CONTRIBUTIONS

DA performed the concluding calculations, prepared the manuscript, and participated in the whole process of manuscript revision; JP and SL performed the simulations. KA, NPA and NP were involved in the project design, supervision of the project and discussion/review of the manuscript.

CONFLICTS OF INTEREST

The authors declare that they have no competing interests.

DATA AVAILABILITY STATEMENT

The data that support the findings of this study are available from the corresponding author, upon reasonable request.

REFERENCES

Azevedo, S., Kaschny, J., de Castilho, C. C., & de Brito Mota, F. (2009). Electronic structure of defects in a boron nitride monolayer. *The European Physical Journal B*, 67(4), 507–512.

Barcza, G., Iv´ady, V., Szilv´asi, T., Voros, M., Veis, L., Gali, A., & Legeza, O. (2021). ´ Dmrg on top of plane-wave kohn–sham orbitals: a case study of defected boron nitride. *Journal of Chemical Theory and Computation*, 17(2), 1143–1154.

Berseneva, N., Gulans, A., Krasheninnikov, A. V., & Nieminen, R. M. (2013). Electronic structure of boron nitride sheets doped with carbon from first-principles calculations. *Physical Review B*, 87(3), 035404.

Cassabois, G., Valvin, P., & Gil, B. (2016). Hexagonal boron nitride is an indirect bandgap semiconductor. *Nature Photonics*, 10(4), 262–266.

Geim, A. K., & Grigorieva, I. V. (2013). Van der waals heterostructures. *Nature*, 499(7459), 419–425.

Giannozzi, P., Andreussi, O., Brumme, T., Bunau, O., Nardelli, M. B., Calandra, M., Car, R., Cavazzoni, C., Ceresoli, D., Cococcioni, M., *et al.* (2017). Advanced capabilities for materials modelling with quantum espresso. *Journal of Physics: Condensed Matter*, 29(46), 465901.

Giannozzi, P., Baroni, S., Bonini, N., Calandra, M., Car, R., Cavazzoni, C., Ceresoli, D., Chiarotti, G. L., Cococcioni, M., Dabo, I., *et al.* (2009). Quantum espresso: a modular and open-source software project for quantum simulations of materials. *Journal of physics: Condensed Matter,* 21(39), 395502.

Kokalj, A. (1999). Xcrysden—a new program for displaying crystalline structures and electron densities. *Journal of Molecular Graphics and Modelling*, 17(3-4), 176–179.

Lin, S., Ye, X., Johnson, R. S., & Guo, H. (2013). First-principles investigations of metal (cu, ag, au, pt, rh, pd, fe, co, and ir) doped hexagonal boron nitride nanosheets: stability and catalysis of co oxidation. *The Journal of Physical Chemistry C*, 117(33), 17319–17326.

Lin, Y., & Connell, J. W. (2012). Advances in 2d boron nitride nanostructures: nanosheets, nanoribbons, nanomeshes, and hybrids with graphene. *Nanoscale,* 4(22), 6908–6939.

Liu, L., Feng, Y., & Shen, Z. (2003). Structural and electronic properties of h-bn. *Physical Review B*, 68(10), 104102.

Liu, Y.-j., Gao, B., Xu, D., Wang, H.-M., & Zhao, J.-x. (2014). Theoretical study on si-doped hexagonal boron nitride (h-bn) sheet: Electronic, magnetic properties, and reactivity. *Physics Letters A,* 378(40), 2989–2994.

MacNaughton, J., Moewes, A., Wilks, R., Zhou, X., Sham, T., Taniguchi, T., Watanabe, K., Chan, C., Zhang, W., Bello, I., *et al.* (2005). Electronic structure of boron nitride single crystals and films. *Physical Review B,* 72(19), 195113.

Novoselov, K. S., Geim, A. K., Morozov, S. V., Jiang, D.-e., Zhang, Y., Dubonos, S. V., Grigorieva, I. V., & Firsov, A. A. (2004). Electric field effect in atomically thin carbon films. *science*, 306(5696), 666–669.

Ooi, N., Rairkar, A., Lindsley, L., & Adams, J. (2005). Electronic structure and bonding in hexagonal boron nitride. *Journal of Physics: Condensed Matter,* 18(1), 97.

Sinthika, S., Kumar, E. M., & Thapa, R. (2014). Doped h-bn monolayer as efficient noble metal-free catalysts for co oxidation: the role of dopant and water in activity and catalytic de-poisoning. *Journal of Materials Chemistry A*, 2(32), 12812–12820.

Xu, M., Liang, T., Shi, M., & Chen, H. (2013). Graphene-like two-dimensional materials. *Chemical reviews*, 113(5), 3766–3798.

Xu, Y.-N., & Ching, W. (1993). Electronic, optical, and structural properties of some wurtzite crystals. *Physical Review B*, 48(7), 4335.